Collective excitations in the metallic triangular antiferromagnet $PdCrO_2$

A. Glamazda, W.-J. Lee, S.-H. Do, and K.-Y. Choi*
Department of Physics, Chung-Ang University, 221 Huksuk-Dong, Seoul 156-756, Republic of Korea

P. Lemmens
Institute for Condensed Matter Physics, TU Braunschweig, D-38106 Braunschweig, Germany

J. van Tol
Department of Chemistry and Biochemistry, Florida State University, Tallahassee, Florida 32306, USA
and National High Magnetic Field Laboratory, Florida State University, Tallahassee, Florida 32310, USA

J. Jeong and H.-J. Noh
Department of Physics, Chonnam National University, Gwangju 500-757, Korea
(Received 3 February 2014; published 18 July 2014)

We report a combined Raman-scattering and electron spin resonance (ESR) study of the metallic triangular compound $PdCrO_2$ along with lattice dynamic calculations. Our Raman data reveal (i) an exponential increase of the 706 cm^{-1} A_g mode involving the out-of-plane motions of the oxygen atoms and (ii) electronic Raman scatterings whose scattering rate is strongly suppressed as the temperature approaches $T_N = 37.5$ K. The temperature dependence of the ESR linewidth is described by a critical broadening $\Delta H_{pp}(T) \propto (T - T_N)^{-p}$ with the exponent $p = 0.63 \pm 0.05$. These are interpreted in terms of coherence of interplane hoppings along the c axis and a reconstruction of electronic bands on approaching T_N. Our results suggest a significant role of an interference between metallic and magnetic layers in explaining collective excitations in $PdCrO_2$.

DOI: 10.1103/PhysRevB.90.045122 PACS number(s): 75.10.Jm, 75.50.Ee, 75.47.Np, 78.30.Er

I. INTRODUCTION

Frustrated quantum spin systems with itinerant degrees of freedom have provided a promising route to achieve novel states of matter such as anomalous Hall effects and emergent gauge fields [1–3]. A prominent example is found in $PdCrO_2$, which is a magnetic counterpart of the metallic delafossite $PdCoO_2$ [4–7].

The interesting properties of $PdCrO_2$ are based on its crystal structure, consisting of alternating stacked layers of Pd and Cr triangular lattices along the c axis [8]. The Pd layers with the large sp-like band dispersions give rise to metallic conductivity, while Cr^{3+} ions in the CrO_2 layer are responsible for localized $S = 3/2$ spin moments [9]. This compound shows an unconventional anomalous Hall effect, whose origin remains elusive [6]. Very recent transport and spectroscopic studies [5,7] have suggested that the interaction of the magnetic structure with conduction electrons is crucial in understanding the anomalous transport properties. However, its influence on collective excitations has not yet been addressed. This motivated us to investigate to what extent lattice and electronic excitations are affected by mutual couplings between localized spin and metallic subsystems. Raman spectroscopy can serve as an experimental tool of choice as it may simultaneously probe lattice anomalies and low-energy electronic excitations. Combined with electron spin resonance (ESR), one can address spin dynamics as well.

$PdCrO_2$ undergoes an antiferromagnetic transition at $T_N = 37.5$ K with a 120° spin structure [10,11]. Very recently, two independent angle-resolved photoemission spectroscopy (ARPES) studies have reported a markedly different electronic structure in the antiferromagnetic phase [5,12]. Sobota *et al.* [12] found no hint of an electronic reconstruction, whereas Noh *et al.* [5] observed folded bands. These seemingly contradicting results are ascribed to the large difference of employed photon energies, leading to the variation of the photoionization cross-section ratio of Cr 3d to Pd 4d. Sobota's ARPES experiment adopting a lower phonon energy predominantly probes the surface state with mostly Pd 4d characters, while Noh's one with a higher phonon energy is highly sensitive to Cr 3d orbitals. The Fermi-surface reconstruction is further supported by de Haas–van Alphen (dHvA) oscillations [7]. These results indicate the substantial hybridization between the conduction electrons and the localized spins in $PdCrO_2$.

The intimate interplay between the spin and the electron subsystem can also account for enhanced spin-fluctuation scattering as well as interplane magnetic interactions mediated by Pd ions [13]. The sudden drop of the resistivity with decreasing temperature through T_N is due to the suppression of magnetic-fluctuation contributions to electron transport [14]. In addition, the magnetic susceptibility data are not typical for two-dimensional spin systems: (i) the proximity of the broad maximum temperature to T_N and (ii) no apparent Curie-Weiss behavior up to 450 K [9,13,15]. This signals the significance of three-dimensional and longer exchange interactions.

In this paper, we investigate lattice and electronic excitations as well as spin dynamics of the metallic triangular compound $PdCrO_2$. We provide spectroscopic evidence that collective excitations are governed by a considerable

*kchoi@cau.ac.kr

interplay between the Cr moments and the metallic electrons.

II. EXPERIMENTAL DETAILS

Single crystals of $PdCrO_2$ were grown by the NaCl flux method described in the literature [8]. For Raman and ESR experiments, crystals with typical dimensions of $1 \times 1 \times 0.1$ mm^3 were used. The samples were installed into a He-cooled closed cycle cryostat with a temperature range of $T = 5$–300 K. The Raman spectra were taken in a (quasi)backscattering geometry with the excitation line $\lambda = 532$ nm of a Nd:YAG (neodymium-doped yttrium aluminium garnet) solid-state laser. The scattered spectra were collected with a triple spectrometer (Dilor-XY-500) and a micro-Raman spectrometer (Jobin Yvon LabRam) equipped with a liquid-nitrogen-cooled CCD. High-frequency ESR experiments were performed at 240 GHz using a quasioptical spectrometer and sweepable 12 T superconducting magnet. The spectrometer employs a superheterodyne detection scheme with a lock-in amplifier for field modulation [16]. Thus, the field derivative of a microwave absorption signal was recorded as a function of a sweeping external field.

III. RESULTS AND DISCUSSION

A. Phonon spectra and lattice dynamical calculations

According to the factor group analysis of the rhombohedral $R\bar{3}m$ space group, one obtains the total irreducible representation for the Raman-active modes $\Gamma = A_{1g}(aa,bb,cc) + E_g(aa,bb,ab,bc,ca)$. To investigate the evolution of optical phonons, we employed a micro-Raman spectrometer. In Fig. 1, we present the temperature dependence of Raman spectra. At $T = 5$ K, we observe two phonon modes at 556 and 710 cm^{-1} in both (xx) and (xy) polarization. The observed phonon number perfectly matches the predicted one. This rules out any crystal symmetry reduction, which may occur due to spin-lattice couplings. However, the weak A_{1g} mode appears in (xy) polarization, possibly due to the leakage of a selection rule. Here we note that the same number of phonon peaks with similar energies at 520 and 712 cm^{-1} has been reported in the sister delafossite compound $PdCoO_2$ [17].

On the basis of the shell-model lattice dynamics, we calculate the Γ-point phonon modes with the GULP package to assign the symmetries and eigenvectors to the observed phonon modes [18]. In this procedure, the interionic interactions are described by long-range Coulomb potentials and short-range Born-Mayer-Buckingham potentials between ions i and j,

$$V_{BM}(r) = A_{ij}\exp(-r/\rho_{ij}) - C_{ij}/r^6,$$

where A_{ij} and ρ_{ij} denote the strength and the range of the repulsive interaction, respectively, and C_{ij} describes

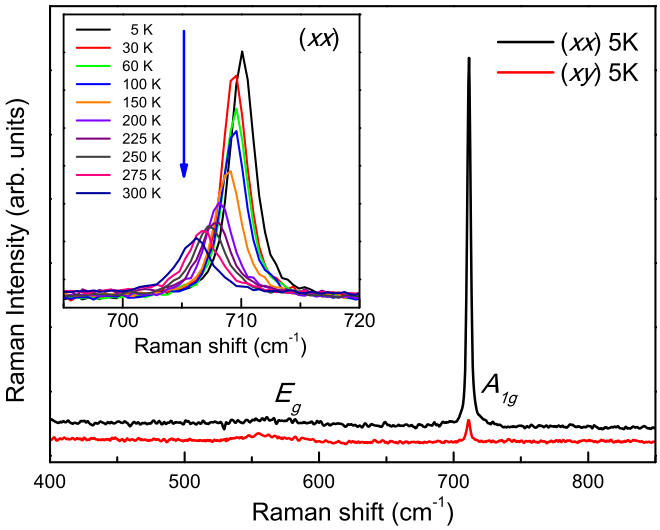

FIG. 1. (Color online) Representative Raman spectrum at $T = 5$ K in (xx) and (xy) polarization. The strong peak at 710 cm^{-1} is assigned to the A_{1g} mode and the weak peak at 556 cm^{-1} to the E_g mode according to the lattice dynamical calculations; see the text for details. Inset: Zoom of the 710 cm^{-1} A_{1g} mode in (xx) polarization as a function of temperature.

an attractive part with the interatomic distance r. Starting from well-documented data, the shell-model parameters are optimized to reach a reasonable agreement with experimental Raman frequencies. The resulting shell-model parameters are summarized in Table I. We compare the observed peak frequencies to the calculated ones in Table II. We find a noticeable discrepancy between them. We ascribe it partly to the failure of describing Pd-Pd metal-metal bonding within the shell model [13]. However, since both modes are well separated in frequencies from each other, we can identify their eigenvectors without ambiguity.

Figure 2 depicts the calculated eigenvectors of the two-phonon modes at $T = 300$ K. The 550 cm^{-1} E_g mode corresponds to in-plane motions of the oxygen atoms, which are in phase within a plane, but are out of phase between the adjacent planes. The 706 cm^{-1} A_{1g} mode involves out-of-phase motions of the oxygen atoms along the c axis. In the in-plane polarizations, the A_{1g} mode shows a pronounced scattering intensity (see Fig. 1). Due to the thinness of the crystal, the interplane polarizations could not be measured and thus the phonon parameters of the E_g mode cannot be examined as a function of temperature.

In the following, we focus on the temperature dependence of the A_{1g} mode as zoomed in the inset of Fig. 1. With decreasing temperature, its scattering intensity is markedly enhanced, its frequency moderately hardens, and its linewidth

TABLE I. List of shell-model parameters for the shell-shell and core-shell interactions.

Atom	X ($\|e\|$)	Y ($\|e\|$)	K (eV/Å)	Atomic pair	A (eV)	ρ (Å)	C (eV Å^6)
Pd	1	0	0	Pd-O	1217.5	0.28	0
Cr	3	0	0	Cr-O	1717.1	0.2947	0
O	0.813	−2.813	74.92	O-O	22764.0	0.149	27.88

TABLE II. List of phonon symmetries and calculated frequencies in cm^{-1} at the Γ point for $PdCrO_2$.

Expt. (cm^{-1})	Cal. (cm^{-1})	Assignment
550	409	E_g (Oxygen, ab motions)
706	653	A_{1g} (Oxygen, $+c$ and $-c$ motions)

slightly narrows. Extracting the phonon parameters by fitting to a Lorentz profile, we detail the temperature dependence of the lattice dynamics. The resulting parameters are plotted in Fig. 3. As the temperature is lowered from room temperature, the 706 cm^{-1} mode undergoes a small hardening by 4 cm^{-1}. Its full width at half maximum (FWHM) decreases monotonically and its scattering intensity exhibits an exponential-like growth.

Based on phonon-phonon decay processes [19], we first try to describe the temperature dependence of the frequency by

$$\omega_{ph}(T) = \omega_0 + A[1 + 2/(e^{\hbar\omega_0/2k_BT} - 1)], \quad (1)$$

where the first term $\omega_0 = 717.6 \pm 0.3$ cm^{-1} is the bare phonon frequency of the A_{1g} mode and the second term with the constant $A = -7.6 \pm 0.2$ cm^{-1} is related to the decay of the optical phonon into two acoustic phonons with the same frequencies and opposite momenta (three-phonon processes). The fitted curve reproduces well the experimental data in nearly the whole temperature range, except for a few points below T_N [see the solid line of Fig. 3(a)]. Next, we adopt the same model to describe the temperature behavior of the FWHM:

$$\Gamma_{ph}(T) = \Gamma(0)[1 + 2/(e^{\hbar\omega_0/2k_BT} - 1)], \quad (2)$$

where $\Gamma(0) = 2.18 \pm 0.05$ cm^{-1} is the positive constant. We find discernible deviation between the experimental data and the fitted curve, as seen from the solid line in Fig. 3(b). The discrepancy between them is somewhat larger than the errors. Given that spin fluctuations contribute to resistivity [14], this may be due to the additional line broadening

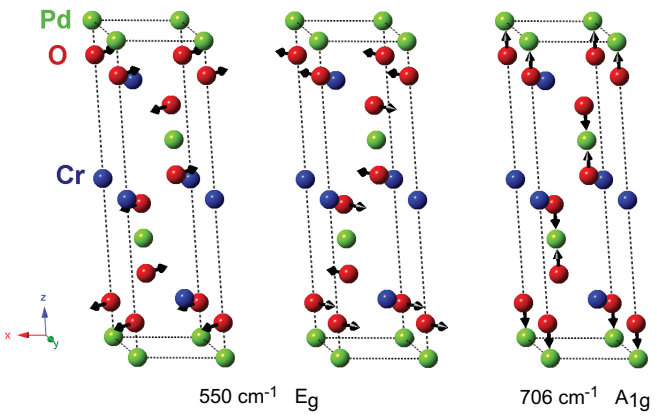

FIG. 2. (Color online) Schematic representation of calculated eigenvectors of the 550 cm^{-1} E_g and the 706 cm^{-1} A_{1g} symmetry mode at room temperature. The amplitude of the vibrations is represented by the arrow length. Green balls stand for Pd ions, red balls for O ions, and blue balls for Cr ions, respectively.

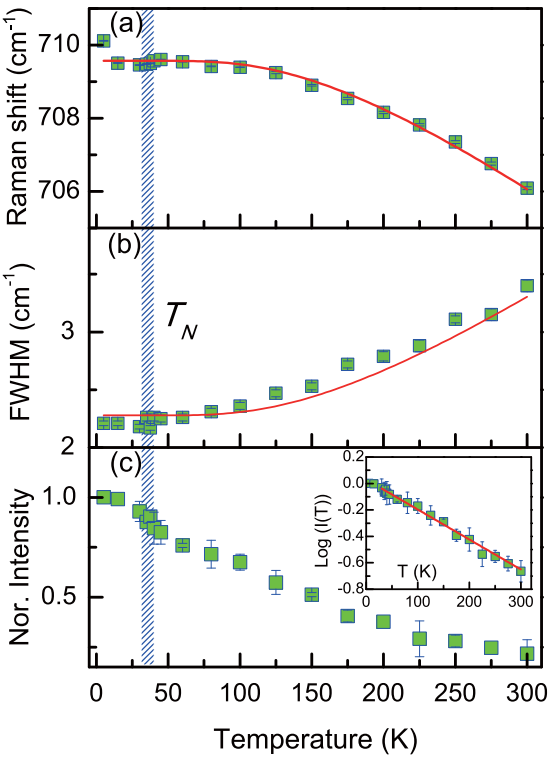

FIG. 3. (Color online) (a) Temperature dependence of the frequency of the 706 cm^{-1} mode. The solid line is a fit to Eq. (1). (b) Temperature dependence of the full width at half maximum. The solid line is a fit to Eq. (2). (c) Temperature dependence of the normalized intensity. The inset plots the normalized intensity on a semilogarithmic scale.

arising from phonon scatterings by magnetic fluctuations. As to the scattering intensity, the normalized integrated intensity $I(T)$ increases by one order of magnitude as the temperature is lowered from 300 to 5 K. As evident from the semilogarithmic plot of $I(T)$ versus T in the inset of Fig. 3(c), the phonon intensity is described by an exponential decay function, $I(T) \propto \exp(-k_BT/\Delta)$ with $\Delta = 440.7 \pm 0.6$ K. The moderate empirical constant Δ indicates the presence of the energy scale at which the phonon scattering process changes.

In general, the Raman-scattering intensity is determined by extrinsic and intrinsic effects. Because the resistivity of $PdCrO_2$ shows a highly metallic behavior [14], the variation of an attenuation length $\delta(T)$ with temperature may be a main source of the extrinsic effect. In this case, the scattered intensity is proportional to $I(T) \sim \exp[-2r/\delta(T)]$. Obviously, this is oppositive to the exponential increase of $I(T)$ with decreasing temperature. This signals that an intrinsic mechanism should be invoked to explain the exponential increase of $I(T)$. It is worth noting that the high-T_c multiferroic compound CuO exhibits a similar phonon anomaly [20]. The exponential behavior of $I(T)$ was discussed in terms of a competition of polar and nonpolar lattice distortions. However, the studied compound shows no hints for lattice anomalies and thus we resort to another mechanism that alters a mode-specific dielectric function. We recall that the integrated intensity of phonons relies on a change of band energy as well as of

interionic distance [21]. In this light, a modification of band energy is responsible for the observed large variation of $I(T)$ because the latter possibility is improbable.

The band reconstruction scenario is supported by the ARPES measurements along with tight-binding calculations, which unravel the idea that in the antiferromagnetic phase, the magnetic hoppings occur in addition to the normal hopping between Pd ions [5]. Since the magnetic hopping is mediated through the conduction electron in the O-Pd-O dumbbells, it leads to the appearance of the folded bands. According to our lattice dynamic calculations, the displacement of the A_{1g} mode involves the out-of-plane motions of the oxygen atoms and thus is intrinsically tied to the magnetic hopping paths. Upon approaching T_N, the magnetic hoppings become coherent along the c axis and the electronic bands become folded. Consequently, the electronic reconstruction changes the A_{1g} vibration from an incoherent to a coherent process, leading to an enhancement of the intensity of the out-of-plane mode.

B. Collision-dominated electronic response

We will turn now to electronic Raman scattering, which extends to high energies of 1600 cm^{-1}. The electronic Raman spectra were measured using a triple spectrometer to have access to a low-frequency region. Figure 4 shows the Bose-corrected Raman response $\mathrm{Im}\,\chi(\omega) = S(\omega)/[1 + n(\omega)]$, where $S(\omega)$ is the raw Raman data and $1 + n(\omega) = 1/[1 - \exp(-\hbar\omega/k_B T)]$. The observed electronic Raman scattering is interpreted in terms of a collision-limited model. Such low-frequency electronic scattering appears in correlated metals or doped semiconductors when the carrier scattering rate is larger than the product of the wave vector and Fermi velocity ($\Gamma_e > q \cdot v_F$), for example, due to inelastic electronic scattering by spins, orbital, impurities, phonons, etc. [22]. In the collision-dominated regime, the Bose-corrected electronic response is given by

$$\mathrm{Im}\,\chi(\omega) \propto \frac{B\omega\Gamma_e}{\omega^2 + \Gamma_e^2}, \tag{3}$$

where B is the symmetry-dependent amplitude and Γ_e is the carrier scattering rate.

To analyze the electronic response quantitatively, $\mathrm{Im}\,\chi(\omega)$ is fitted to Eq. (3). As seen from the presentative fits at $T = 5$, 100, and 240 K in the solid lines of Fig. 4, the employed model gives a reasonable description of the electronic background. The small deviations are due to one-phonon excitations between 500 and 900 cm^{-1} as well as to two-phonon excitation at 1097 cm^{-1}. The temperature dependence of the scattering rate $\Gamma_e(T)$ is summarized in the inset of Fig. 4.

For a simple metal, a possible electronic response is given by a high-energy plasmonlike excitation. If the metallic electrons of the Pd layers are decoupled from the Cr spins, we expect no pronounced low-energy electronic response. In this sense, the observed electronic response indicates that the metallic electrons of the Pd layers are scattered from the Cr spins. This is consistent with the dHvA and ARPES measurements [5,7], which demonstrate the intrinsic coupling between two subsystems. Here we note that the collision-dominated scatterings arising from spin polarons and/or spin fluctuations have been previously reported for the layered cobaltates Na_xCoO, colossal magnetoresistance manganites, and ferromagnetic semiconductors $Eu_{1-x}Gd_xO$ [23–25].

With decreasing temperature, the maximum position of $\mathrm{Im}\,\chi(\omega)$ shifts toward lower energies, while its scattering intensity hardly varies with temperature. The former is related to the scattering rate Γ_e, while the latter to the amplitude B. As shown in the inset of Fig. 4, $\Gamma_e(T)$ decreases gradually with decreasing temperature and then drops abruptly at T_N. The drop of $\Gamma_e(T)$ is beyond the errors. Remarkably, we find the resemblance between $\Gamma_e(T)$ and the resistivity due to the magnetic scattering (compare the inset of Fig. 4 with Fig. 2 of Ref. [9]). The decreasing scattering rate toward low temperatures would then be ascribed to a suppression of spin fluctuations, while developing the short-range spin correlation above T_N, and, finally, the long-range antiferromagnetic order at T_N. The temperature-independent scattering intensity may be explained by the fact that the decrease of $\Gamma_e(T)$ is largely compensated by the increase of conductivity.

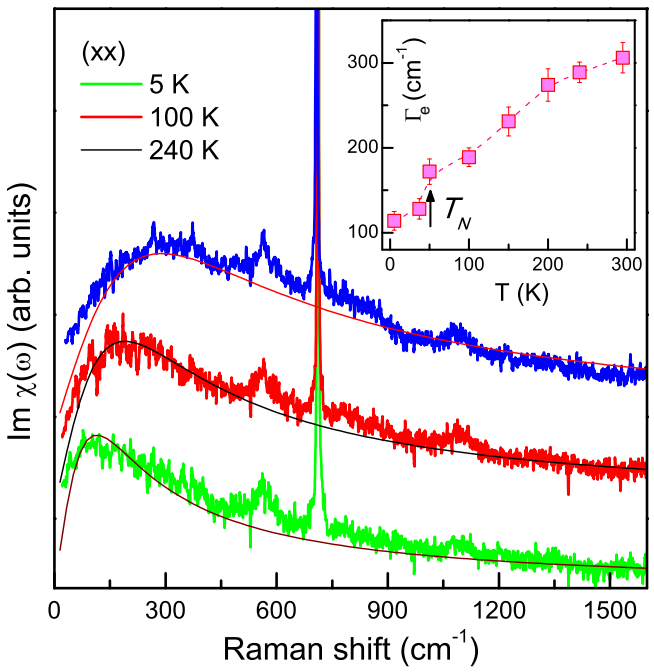

FIG. 4. (Color online) Bose-corrected Raman spectra $\mathrm{Im}\,\chi(\omega)$ at $T = 5$, 100, and 240 K. The Raman responses are vertically shifted for clarity. The solid lines are fits to Eq. (3). The inset plots the scattering rate $\Gamma_e(T)$ as a function of temperature.

C. Electron spin resonance

To obtain information on the development of local spin correlations, we performed high-frequency ESR at $\nu = 240$ GHz. Figure 5(a) displays the temperature dependence of the ESR signals for the $H \perp ab$ plane. At $T = 220$ K, we observe a single Lorentzian line, which originates from paramagnetic Cr^{3+} ions. The exchange-narrowed resonance line occurs due to fast electronic fluctuations induced by a strong antiferromagnetic interaction between the Cr^{3+} ions. The g factor is determined by the relation $g_{ab} = h\nu/\mu_B H_{\mathrm{res}} = 1.985 \pm 0.003$, where μ_B is the Bohr magneton and $H_{\mathrm{res}} = 8.6376 \pm 0.0002$ T is

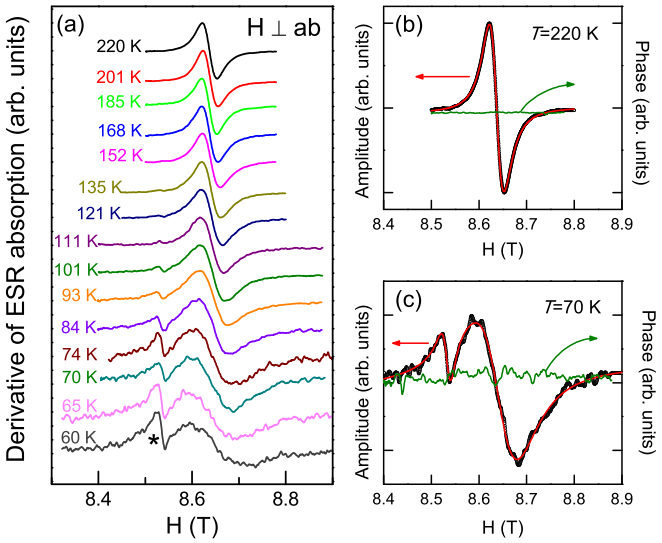

FIG. 5. (Color online) (a) Derivative of the ESR absorption spectra of the $PdCrO_2$ crystal measured at $\nu = 240$ GHz for the $H \perp ab$ plane as a function of temperature. The spectra are vertically shifted for clarity. The asterisk denotes an impurity signal. Representative fits of the amplitude of the ESR signal to Lorentzian profiles at (b) $T = 220$ K and (c) $T = 70$ K are shown together with their phase.

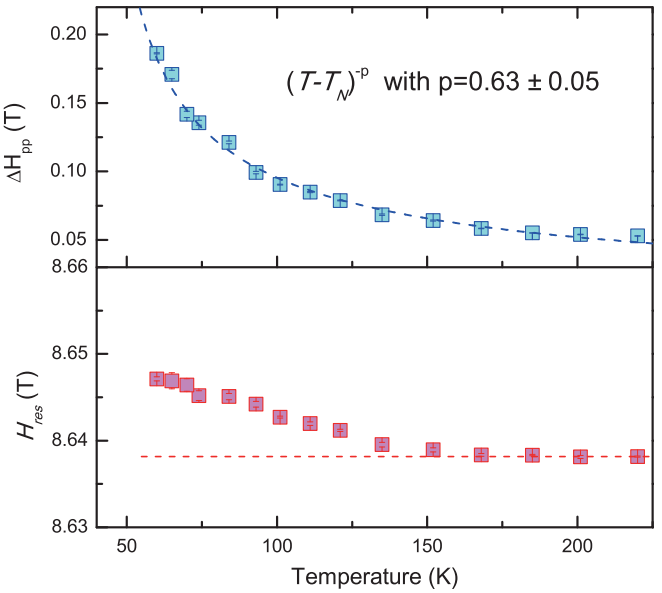

FIG. 6. (Color online) Upper panel: Temperature dependence of the ESR linewidth $\Delta H_{pp}(T)$. The dashed line is a fit to a power law. Lower panel: Temperature dependence of the resonance field $H_{\rm res}(T)$. The dashed line is a guide to the eye.

the resonance field. The determined g value is typical for a less-than-half-filled ion with a quenched orbital moment.

With decreasing temperature, the spectra become broader and finally wiped out in the vicinity of T_N. Noticeably, the weak, sharp peak at $H_{\rm res} = 8.5342 \pm 0.0007$ T (denoted by the asterisk) starts to appear at $T^* = 135$ K. The corresponding g factor of the extra peak is found to be $g = 2.009 \pm 0.004$ and is independent of temperature. Thus, it is ascribed to a few percentages of defects and orphan spins, which are sensitive to ESR. To quantify the evolution of spin dynamics, the resonance field ($H_{\rm res}$) and the peak-to-peak linewidth (ΔH_{pp}) are extracted by fitting to a Lorentzian profile. In Figs. 5(b) and 5(c), we present the presentative fits of the ESR signal to Lorentzian profiles at $T = 220$ and 70 K, respectively. Here we stress that the adopted superheterodyne detection scheme allows a separation of the absorption and dispersion part of the complex resonance response [16]. Combined with a lock-in technique, both $H_{\rm res}$ and ΔH_{pp} can be determined very accurately, compared to an absorption-type spectrometer. The resulting ESR parameters are plotted in Fig. 6.

For temperatures above 150 K, $H_{\rm res}(T)$ is temperature independent and then $H_{\rm res}(T)$ starts to increase appreciably upon cooling from 150 K. The sizable increase of $H_{\rm res}(T)$ for temperatures much higher than T_N is ascribed to the development of internal fields due to short-range ordering. Noticeably, the distorted $S = 3/2$ triangular antiferromagnet α-$CaCr_2O_4$ having $T_N = 42.6$ K and $\Theta_{CW} \sim 564$ K shows a sizable shift of $H_{\rm res}(T)$ for temperatures below 100 K [26]. Since $PdCrO_2$ and α-$CaCr_2O_4$ have the similar magnetic ordering temperature and the Curie-Weiss temperature [15], the observed upshift of $H_{\rm res}(T)$ is an intrinsic feature of frustrated magnets.

The temperature dependence of the linewidth is given by $\Delta H_{pp}(\theta,T) = \alpha(\theta,T)\Delta H_{pp}(\theta,\infty)$, where $\Delta H_{pp}(\theta,\infty)$ is the linewidth in an uncorrelated paramagnetic limit. A T-independent linewidth is characteristic of an infinite-temperature, paramagnetic state. As the temperature is lowered from 220 K, $\Delta H_{pp}(T)$ exhibits a critical-like broadening. This is ascribed to the development of short-range spin correlations, which is consistent with the formation of an internal field in a similar temperature range. The persistence of strong spin correlations up to the Curie-Weiss temperature is a hallmark of frustrated magnets. This means that our system does not reach the pure paramagnetic regime at room temperature.

The line broadening is fitted to a critical power law, $\Delta H_{pp}(T) \propto (T - T_N)^{-p}$, with the exponent $p = 0.63 \pm 0.05$ (see the dashed line in the upper panel of Fig. 6). The obtained critical exponent is found to lie between the value of $p = 0.7$–0.9 reported in the $S = 3/2$ triangular antiferromagnets $ACrO_2$ (A = Li, Na, Cu, and Ag) and that of $p \approx 0.39$–0.48 in the distorted $S = 3/2$ triangular antiferromagnet α-$CaCr_2O_4$ [26–28]. The large variation of the critical exponent among the same class of spin systems seems to be due to the presence of another spin-relaxation channel.

Lastly, we mention that the triangular Heisenberg antiferromagnet has been proposed to undergo a Kosterlitz-Thouless (KT)-like transition with Z_2 vortices, which are related to the vector chirality defined by the 120° spin structure. Magnetic vortices have been invoked to explain the ESR linewidth in the Cr-based triangular antiferromagnets $ACrO_2$ [27,28]. In a paramagnetic regime, the vortex model describes $\Delta H_{pp}(T)$ equally well as the critical broadening does. Nonetheless, the direct experimental observation of a vortex melting lacks because an ESR signal is wiped out well above T_N due to fast fluctuating spins. In our compound, the wipe out occurs already at $T = 1.5T_N$ because of enhanced hybridization of the Cr spins to the conduction electrons. The magnetic vortex, if present, will be destroyed by the interplane hopping electrons.

IV. CONCLUSION

In summary, we have presented a combined Raman-scattering and ESR study of the metallic triangular compound $PdCrO_2$ together with lattice dynamic calculations. In first approximation, conductivity and magnetism originate from separate Pd and Cr layers. However, our results show a significant role of the interplay between Cr moments and the conduction electrons in explaining low-energy electronic scatterings and anomalies of the out-of-plane oxygen mode at 706 cm^{-1}. In particular, the decrease of an electron scattering rate and the exponential increase of a phonon intensity, as the temperature approaches T_N, are interpreted in terms of coherence of interplane hoppings along the c axis and a suppression of spin fluctuations. In addition, the critical ESR line broadening suggests the predominance of correlated spin fluctuations over a wide temperature range. $PdCrO_2$ provides a unique opportunity to study an interference between metallic and magnetic layers in a single bulk system.

ACKNOWLEDGMENTS

This work was supported by Korea NRF Grants No. 2009-0093817, No. 2010-0011325, No. 2012-046138, and No. 2012M2B2A4029607, and by NTH School "Contacts in Nanosystems" and DFG-RTG 1953/1, Nanomet/B-IGSM. A portion of this work was performed at the National High Magnetic Field Laboratory, which is supported by National Science Foundation Cooperative Agreement No. DMR-1157490, the State of Florida, and the US Department of Energy.

[1] N. Nagaosa, J. Sinova, S. Onoda, A. MacDonald, and N. Ong, Rev. Mod. Phys. **82**, 1539 (2010).
[2] Q. Si, Physica B: Condens. Matter **378–380**, 23 (2006).
[3] S. Onoda and Y. Tanaka, Phys. Rev. Lett. **105**, 047201 (2010).
[4] Han-Jin Noh, Jinwon Jeong, Jinhwan Jeong, En-Jin Cho, Sung Baek Kim, Kyoo Kim, B. I. Min, and Hyeong-Do Kim, Phys. Rev. Lett. **102**, 256404 (2009).
[5] Han-Jin Noh, Jinwon Jeong, Bin Chang, Dahee Jeong, Hyun Sook Moon, En-Jin Cho, Jong Mok Ok, Jun Sung Kim, Kyoo Kim, B. I. Min, Han-Koo Lee, Jae-Young Kim, Byeong-Gyu Park, Hyeong-Do Kim, and Seongsu Lee, Sci. Rep. **4**, 3680 (2014).
[6] H. Takatsu, S. Yonezawa, S. Fujimoto, and Y. Maeno, Phys. Rev. Lett. **105**, 137201 (2010).
[7] Jong Mok Ok, Y. J. Jo, Kyoo Kim, T. Shishidou, E. S. Choi, Han-Jin Noh, T. Oguchi, B. I. Min, and Jun Sung Kim, Phys. Rev. Lett. **111**, 176405 (2013).
[8] Hiroshi Takatsu and Yoshiteru Maeno, J. Cryst. Growth **312**, 3461 (2010).
[9] H. Takatsu, H. Yoshizawa, S. Yonezawa, and Y. Maeno, Phys. Rev. B **79**, 104424 (2009).
[10] M. Mekata, T. Sugino, A. Oohara, Y. Oohara, and H. Yoshizawa, Physica B **213–214**, 221 (1995).
[11] E. Rastelli and A. Tassi, J. Appl. Phys. **81**, 4143 (1997).
[12] J. A. Sobota, K. Kim, H. Takatsu, M. Hashimoto, S.-K. Mo, Z. Hussain, T. Oguchi, T. Shishidou, Y. Maeno, B. I. Min, and Z.-X. Shen, Phys. Rev. B **88**, 125109 (2013).
[13] K. P. Ong and D. J. Singh, Phys. Rev. B **85**, 134403 (2012).
[14] H. Takatsu, S. Yonezawa, C. Michioka, K. Yoshimura, and Y. Maeno, J. Phys.: Conf. Ser. **200**, 012198 (2010).
[15] J. P. Doumerc, A. Wichainchai, A. Ammar, M. Pouchard, and P. Hagenmuller, Mater. Res. Bull. **21**, 745 (1986).
[16] J. van Tol, L.-C. Brunel, and R. J. Wylde, Rev. Sci. Instrum. **76**, 074101 (2005).
[17] Hiroshi Takatsu, Shingo Yonezawa, Shinichiro Mourt, Satoru Nakatsuji, Koichiro Tanaka, and Yoshiteru Maeno, J. Phys. Soc. Jpn. **76**, 104701 (2007).
[18] G. D. Gale, J. Chem. Soc., Faraday Trans. **93**, 629 (1997).
[19] M. Balkanski, R. F. Wallis, and E. Haro, Phys. Rev. B **28**, 1928 (1983).
[20] K.-Y. Choi, W.-J. Lee, A. Glamazda, P. Lemmens, D. Wulferding, Y. Sekio, and T. Kimura, Phys. Rev. B **87**, 184407 (2013).
[21] E. Ya. Sherman, O. V. Misochko, and P. Lemmens, in *Spectroscopical Studies of High Temperature Superconductors*, edited by N. M. Plakida (Gordon Breach, London, 2001), Chap. 2.
[22] A. Zawadowski and M. Cardona, Phys. Rev. B **42**, 10732 (1990).
[23] P. Lemmens, V. Gnezdilov, G. J. Shu, L. Alff, C. T. Lin, B. Keimer, and F. C. Chou, Phys. Rev. B **88**, 195151 (2013).
[24] K.-Y. Choi, P. Lemmens, G. Guntherodt, M. Pattabiraman, G. Rangarajan, V. P. Gnezdilov, G. Balakrishnan, D. McK. Paul, and M. R. Lees, J. Phys.: Condens. Matter **15**, 3333 (2003).
[25] H. Rho, C. S. Snow, S. L. Cooper, Z. Fisk, A. Comment, and J.-Ph. Ansermet, Phys. Rev. Lett. **88**, 127401 (2002).
[26] Dirk Wulferding, Kwang-Yong Choi, Peter Lemmens, Alexey N. Ponomaryov, Johan van Tol, A. T. M. Nazmul Islam, Sandor Toth, and Bella Lake, J. Phys.: Condens. Matter **24**, 435604 (2012).
[27] M. Hemmida, H.-A. Krug von Nidda, N. Buttgen, A. Loidl, L. K. Alexander, R. Nath, A. V. Mahajan, R. F. Berger, R. J. Cava, Yogesh Singh, and D. C. Johnston, Phys. Rev. B **80**, 054406 (2009).
[28] Mamoun Hemmida, Hans-Albrecht Krug Von Nidda, and Alois Loidl, J. Phys. Soc. Jpn. **80**, 053707 (2011).